XLVI CILAMCE
VITÓRIA - ES - BRAZIL - 2025
XLVI IBERO-LATIN AMERICAN CONGRESS ON COMPUTATIONAL METHODS IN ENGENEERING

Finite Element-Based Dynamic Analysis of a Hybrid Sounding Rocket During Key Flight Stages

Davi T. da Costa[1], Sergio H. S. Carneiro[1]

[1]*College of Science and Technology in Engineering (FCTE), University of Brasília (UnB)*
Gama Campus, 72444-240, Federal District, Brazil
Dtcbsb@gmail.com, shscarneiro@unb.br

Abstract. This work presents a computational structural dynamic analysis of a hybrid sounding rocket developed at the University of Brasília (UnB), aiming to investigate the vibrational response of the structure during different stages of flight. The analysis focuses on three key structural regions: the base of the payload section, the oxidizer tank platform, and the nozzle interface, areas of critical importance due to their exposure to dynamic loads and their roles in load transmission.

The rocket was modeled in three dimensions using the finite element method within the ANSYS environment, incorporating realistic geometry and material properties. Three flight scenarios were simulated to account for changes in propellant mass over time and their effects on natural frequencies and dynamic amplification. Thrust profiles were based on experimental data obtained during a hybrid motor test conducted in the university's propulsion laboratory.

Modal analysis was conducted to identify the main vibration modes and their associated frequencies, followed by transient simulations to assess acceleration responses under realistic, time-varying thrust loads. Rigid-body and elastic contributions were analyzed separately, with different damping ratios considered. The results provide insight into the structural behavior under operational conditions, supporting the safe design of academic aerospace vehicles.

Keywords: Rocket, Payload, Modal analysis, Thrust, Computational simulation.

1 Introduction

Space launch vehicles experience extreme dynamic loads during ascent, with thrust-induced vibrations posing critical challenges to structural integrity and payload safety. These vibrations can be effectively predicted and mitigated through modal analysis and FEM. Computational simulations enable identification of critical vibration modes and optimization of damping systems, enhancing structural stability as stablished by Meirovitch [1]. Advanced materials, vibration isolators, and active control systems have proven effective in reducing dynamic impacts as shown in Preumont [2] works.

This study employs FEM in ANSYS to evaluate the vibrational behavior of a hybrid-propellant sounding rocket under transient thrust conditions, focusing on three flight phases: ignition, steady-state ascent, and post-burnout. The numerical model is based on a real sounding rocket developed at the University of Brasília, incorporating realistic mass distribution, fuel consumption effects, and concentrated subsystem loads.

The results provide insights into thrust-induced vibration propagation, particularly in sensitive regions such as the payload platform, oxidizer tank interface, and nozzle mount. This analysis contributes to structural design refinement for academic launch vehicles, supporting improved vibration suppression, component durability and subsystem isolation. While focused on uncrewed systems, the methodology may inform future human-rated platforms, where vibration exposure remains a critical factor for both structural and physiological performance.

2 Methods

2.1 Finite element model

The dynamic analysis in this work was based on the structural model of the Circe rocket, an experimental hybrid vehicle developed at the University of Brasília, as illustrated in Fig. 1. The model was built in ANSYS Workbench using geometry and material data from previous flight prototypes. Special attention was given to regions with concentrated mass and significant load transfer, such as the nozzle interface, internal platforms, and oxidizer tank, due to their critical role in vibration transmission.

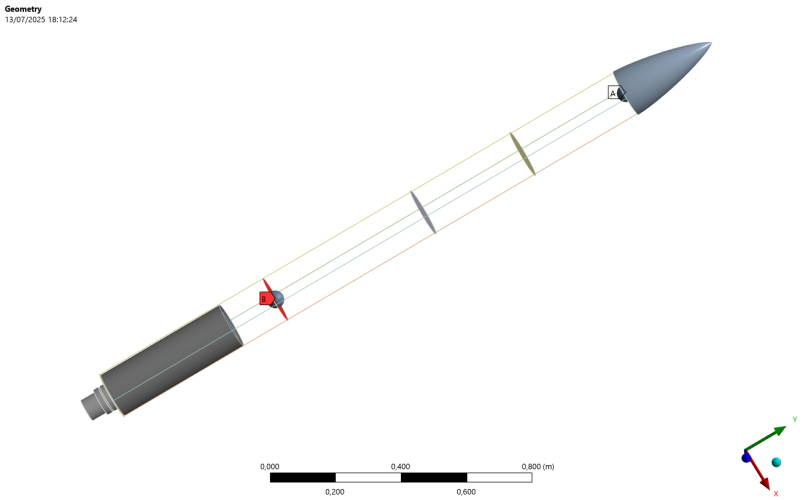


Figure 1. Finite element model without the external fuselage

The rocket was discretized using a multi-element strategy tailored to the mechanical behavior of each component. The fiberglass fuselage, internal platforms, and paraffin-filled fuel tank were modeled with SHELL181 elements to represent their thin-walled nature. Aluminum beams and cylindrical supports were defined using BEAM188 elements, suitable for capturing bending and axial deformation in slender structures. The steel nozzle was modeled with SOLID186 elements, accounting for its volumetric inertia and the interaction between rigid components. Material properties were assigned from datasheets and literature, treating fiberglass and aluminum as isotropic. The mesh was refined in regions of important force trasnmission, particularly near interfaces such as the nozzle, to ensure convergence and capture of high-frequency modes. To include the inertial effects of key components, two concentrated point masses were added: one at the payload platform and another at the oxidizer tank, representing subsystem weights based on engineering data.

2.2 Simulation setup

The global coordinate system was defined with the rocket's longitudinal axis aligned to the global Y-axis, and the X and Z axes defining the lateral direction, ensuring that thrust was applied along the primary axis of symmetry and structural stiffness. The model was considered a free-free object, neglecting interactions with any launch ramp during ignition. The translational and rotational degrees of freedom were restricted through means of exclusion of the rigid-body frequencies during transient analysis.

Two structural configurations were considered: a pre-burn state with full paraffin fuel, used for ignition and steady-flight simulations, and a post-burnout state, with the paraffin removed, representing the final flight stage. This setup enabled assessment of fuel consumption effects on dynamic behavior, particularly changes in inertia and natural frequencies.

Thrust profiles were based on static motor test data performed by Chemical Propulsion Laboratory, University of Brasília [3], as shown in Fig. 2, and processed in MATLAB to generate time-varying thrust curves representing ramp-up, steady combustion, and burnout. These were applied as axial forces on the nozzle face along the Y-axis and uniformly distributed over the contact area. To ensure an uniform distribution of forces, the thrust was applied in an axyssimetrical mesh.

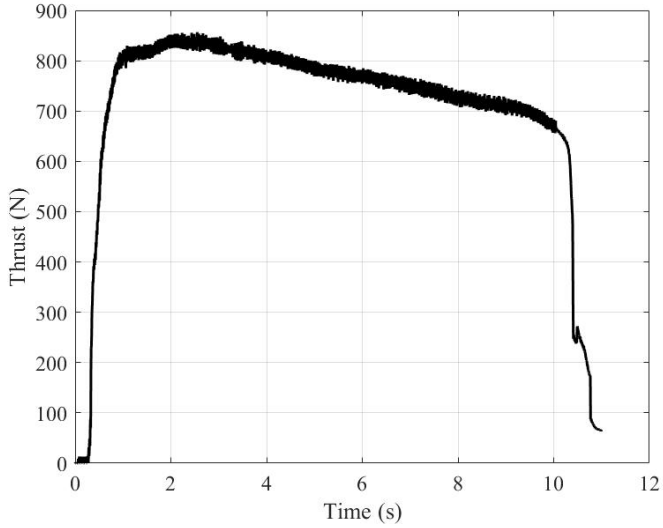


Figure 2. SARA hybrid engine used in the static firing test, with a measured average thrust of 754.64N

Modal analysis was performed on both configurations to extract natural frequencies and associated mode shapes up to approximately 1500 Hz. The solution retained all structural modes within this range, and rigid-body modes were separated from elastic ones using ANSYS built-in filters. Particular focus was given to low-frequency modes, as these were observed in the solution files to be the most likely to be excited by engine-induced loads. The analysis revealed a downward shift in the fundamental frequency when the internal fuel mass was present.

The transient response was computed using the modal superposition method, which allows for efficient integration of the equations of motion using only the most significant vibration modes as stated by N and Govindaraju [4]. A set of 200 modes was retained in the expansion, corresponding to the frequency cutoff established in the modal step. Acceleration responses were extracted from three representative locations: the payload platform, the oxidizer tank support, and the nozzle connection to the fuselage. These nodes were selected based on their functional sensitivity and role in transmitting dynamic loads between structural subsystems. The loads applied during the simulations were extracted from the forces shown in Fig. 2, corresponding to three 1-second intervals: from 0 to 1 seconds, from 2 to 3 seconds, and from 10 to 11 seconds, which were used to define the loading conditions for the transient analysis. A summary of cases analyzed including damping, mode types, flight phases, and measurement points is provided in Table 1.

Table 1. Summary of analyzed cases with measurement points

Undamped Cases			
Mode Type	Flight Phases	Points	Axes
Elastic, Rigid Body	Liftoff Sustained flight Post-burnout	Nose Cone N_2O Tank Nozzle	X, Y, Z
Damped Cases			
Mode Type	Flight Phases	Points	Axes
Elastic only	Liftoff Sustained flight Post-burnout	Nose Cone N_2O Tank Nozzle	X, Y, Z

To simulate energy dissipation, Rayleigh damping was introduced using calibrated α and β coefficients to

approximate structural damping behavior. Damping ratios of 0.005, 0.01, 0.02, 0.03, 0.05, and 0.1 were tested, covering typical ranges for aerospace materials, including composites and metals, as stated by Riso et al. [5]. Simulations were executed over 1 s intervals with a time step of 5×10^{-3} s, capturing the full duration of dynamic excitation in each flight phase.

3 Results and discussion

3.1 Modal Analysis

A modal analysis was conducted to determine the rocket's natural frequencies and mode shapes. The structure was modeled under free-free boundary conditions, with point masses representing the payload (5 kg) and nitrous oxide tank (20 kg). Additional cases with tank masses of 10 kg, 18 kg, and 17 kg were analyzed to reflect different fuel burn stages.

The first step in the analysis was to define the locations for the point masses, once the mass locations were set, simulations were performed with as many modes as computational resources would allow. The participation factor of each mode was then analyzed, and the most relevant modes for the rocket's dynamic behavior were selected. The modal analysis results are critical for the subsequent transient response analysis, as these modes will guide the prediction of the rocket's behavior under dynamic conditions as seen in similar works such as Rosso et al. [6].

The natural frequencies ranged from 43.36 Hz to 1500 Hz. The lowest-frequency modes, such as those at 43.36 Hz (illustrated in Fig. 3), 110.98 Hz, and 134.4 Hz, had the highest participation factor. Configurations with reduced fuel, such as the 10 kg case without paraffin, exhibited higher natural frequencies, indicating a lower susceptibility to resonance in certain flight conditions. Conversely, the inclusion of paraffin reduced the frequencies due to the increased mass and modified material distribution. These observations underscore the importance of accurately modeling fuel mass to ensure realistic predictions of the rocket's dynamic behavior.

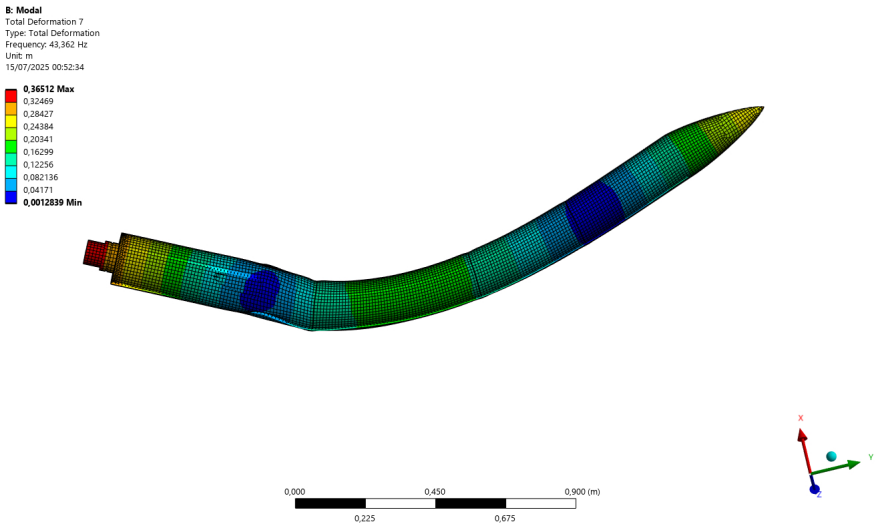


Figure 3. First Bending Mode (43.362 Hz)

3.2 Transient Response Analysis

This section presents the rocket's dynamic behavior under real thrust loading, using a transient simulation informed by test-derived thrust curves. Acceleration responses were evaluated at the payload, oxidizer tank platform, and nozzle base, across the x, y, and z directions. These results were evaluated for different model configurations, including purely elastic modal bases and extended modal bases including rigid body modes, with and without the influence of the internal fuel mass. A summary of these results is displayed in Table 2.

Table 2. Acceleration RMS (and Peak) values for different axes at key points (m/s²)

Phase	**Point**	**X**	**Y**	**Z**
Liftoff	Nose Cone	0.00043 (0.00150)	1.0668 (3.349)	0.00046 (0.00128)
	N_2O Tank	0.00042 (0.00140)	0.6604 (1.9396)	0.00030 (0.00074)
	Nozzle Interface	0.00120 (0.00404)	0.2824 (0.86876)	0.00097 (0.00353)
Sustained Flight	Nose Cone	0.00440 (0.01607)	8.1885 (27.184)	0.00469 (0.01469)
	N_2O Tank	0.00366 (0.01263)	4.5072 (13.723)	0.00323 (0.00839)
	Nozzle Interface	0.01002 (0.03328)	2.1038 (5.2674)	0.00914 (0.03096)
Post-burnout	Nose Cone	0.00307 (0.00832)	4.3904 (12.174)	0.00327 (0.00767)
	N_2O Tank	0.00419 (0.01203)	4.1567 (11.036)	0.00380 (0.00839)
	Nozzle Interface	0.00751 (0.01849)	1.6299 (4.2921)	0.00748 (0.01756)

During the first second of simulation, corresponding to liftoff, the rocket transitions from static equilibrium to a dynamic regime, with thrust rapidly exceeding 800 N. This impulsive excitation activates high-frequency elastic modes, resulting in significant acceleration peaks throughout the structure. While the force acts primarily along the y axis, small oscillations in the x and z directions indicate structural asymmetries and modal coupling. In contrast, y-axis accelerations are substantially higher—exceeding 3 m/s² at the payload interface and surpassing 20 m/s² when rigid body modes are included—reflecting the translational motion of the entire structure.

In the steady-flight regime (2-3 s), thrust stabilizes between 830 and 850 N, yielding a distinct response pattern. Acceleration peaks decrease in some regions due to the damping effect of the paraffin mass, while oscillations become more persistent and harmonic. In the x direction, accelerations reach up to 0.02 m/s²—modest but potentially relevant to lateral stability. In the y direction, as shown in Fig. 4, the payload initially experiences accelerations near 3g, which progressively diminish as the paraffin acts as added inertia and passive damping. A similar trend is observed in the z direction, with initial spikes followed by steady decay. The symmetric response across transverse axes suggests more uniform excitation and longitudinal propagation of vibratory energy. Including rigid body modes, longitudinal acceleration stabilizes around 22 m/s², peaking at 48 m/s², representing the net inertial motion during powered ascent.

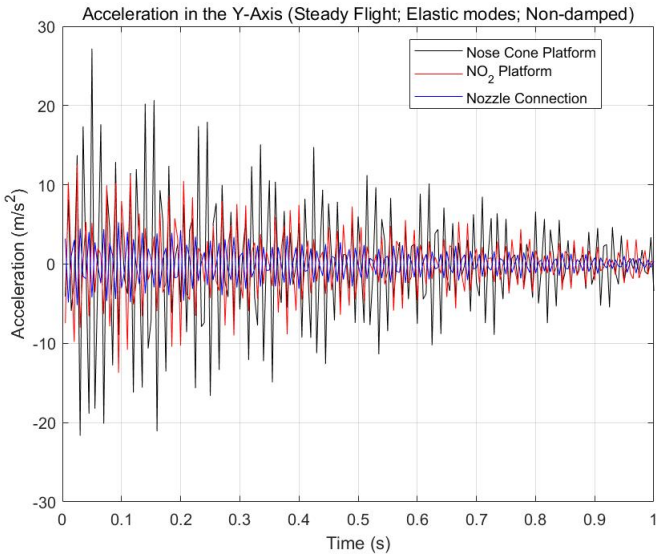


Figure 4. Acceleration Response in Steady-Flight phase, Y-Axis

In the final phase (10-11 s), motor shutdown leads to a sharp thrust drop and excitation from abrupt load variation. This deceleration phase triggers natural frequencies not dominant during powered flight. Now in bal-

listic motion, the rocket exhibits free vibrations shaped by local stiffness and inertia. The structure behaves more uniformly across monitored regions: transverse accelerations persist at low amplitude, while y-axis acceleration decays more noticeably due to the loss of primary excitation. Compared to earlier phases, reduced peak loads lead to smoother energy dissipation and a milder vibrational response. Rigid body contributions reveal residual longitudinal accelerations from the prior phase, quickly decaying to around 3 m/s² in the y direction, consistent with inertial motion in ballistic flight.

3.3 Damping Effects on Transient Response

In this stage, the transient structural response of the rocket was examined under structural damping. The same loading conditions from the undamped case were retained, with damping ratios $\zeta = 0.005, 0.01, 0.02, 0.03, 0.05$ and 0.1. Rayleigh damping was used, with calibrated coefficients ensuring proportional damping across the frequency range of interest.

Damping significantly reduced both the amplitude and duration of the response. Peak accelerations declined steadily with increasing ζ: during full thrust, vertical acceleration at the nose cone dropped from over 26 m/s^2 (undamped) to around 7 m/s^2 for $\zeta = 0.1$. Lateral accelerations in critical regions such as the platform and fuel tank were similarly attenuated. Damping not only reduced peaks but also shortened post-impulse oscillations.

While peak values illustrate extreme loads, a fuller understanding requires RMS acceleration analysis, shown in Fig. 5. RMS captures cumulative vibrational energy, which is critical in aerospace systems where sustained oscillations can lead to fatigue, degradation, or malfunction.

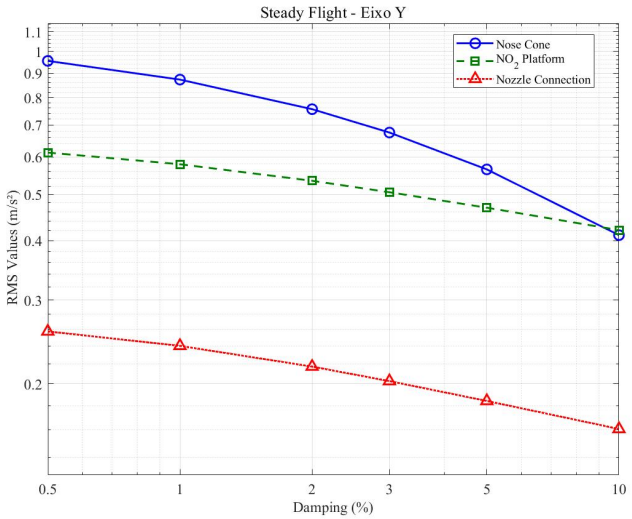


Figure 5. RMS X Zeta in the steady-state combustion phase, Y-Axis

As expected, higher damping led to lower RMS values, indicating greater energy dissipation and reduced vibrational persistence. For example, RMS vertical acceleration at the second platform declined markedly from $\zeta = 0.005$ to $\zeta = 0.1$, confirming damping's role in mitigating sustained loads.

The implications extend beyond structural concerns. Aerospace electronics must operate within strict vibrational limits, as even low-level oscillations may cause connector wear, signal disruption, or guidance errors. Thus, RMS trends inform both structural and subsystem mounting strategies. Additionaly, RMS distributions showed spatial homogenization at higher damping levels. Differences between central and distal regions narrowed, indicating suppression of localized modes and modal coupling. In highly damped cases, RMS values converged across the fuselage, reinforcing the value of damping integration for vibrational resilience.

In summary, the introduction of damping had a decisive impact on both peak and RMS accelerations, with clear benefits in terms of structural longevity, onboard system integrity, and dynamic load predictability. These findings reinforce the necessity of including damping considerations early in the design phase, not only to avoid underestimating vibrational risks but also to guide the optimal allocation of materials, structural reinforcements, and sensitive payload components. A summary of damped acceleration results is displayed in Table 3.

Table 3. Y-axis Acceleration RMS (and Peak) values for different damping coefficients at key points (m/s²)

Phase	**Point**	$\zeta = 0{,}005$	$\zeta = 0{,}03$	$\zeta = 0{,}10$
Liftoff	Nose Cone	0.95505 (3.17220)	0.67507 (2.47560)	0.41078 (1.53180)
	N_2O Tank	0.61265 (1.85640)	0.50563 (1.54710)	0.42084 (1.38020)
	Nozzle Interface	0.25770 (0.82874)	0.20260 (0.68243)	0.16069 (0.53066)
Sustained Flight	Nose Cone	7.02266 (26.39400)	4.48891 (22.77900)	2.56543 (15.29000)
	N_2O Tank	3.86860 (12.93900)	2.50600 (11.65900)	1.58795 (9.78070)
	Nozzle Interface	1.81110 (5.11420)	1.17217 (4.83480)	0.72377 (4.27230)
Post-burnout	Nose Cone	3.86271 (11.98600)	2.61105 (11.09100)	1.63563 (9.35700)
	N_2O Tank	3.65296 (10.88800)	2.45834 (10.17900)	1.52269 (8.43600)
	Nozzle Interface	1.43307 (4.26830)	0.96673 (4.15240)	0.60874 (3.85190)

4 Conclusions

This study highlights the significant role of elastic modes in the dynamic response of the small-scale rocket, especially during takeoff, powered flight, and post-burnout phases. Peak accelerations occur at the nose cone and tank attachment points, with structural flexibility impacting dynamics, particularly during powered flight, where energy transfer and coupling between sections amplify oscillations. The decaying vibrations during end-of-burn phase confirm the model's physical validity, with mild oscillations in regions with low energy dissipation.

While rigid body modes result in higher accelerations, their temporal profile mirrors the thrust curve in the y direction, reflecting the rocket's global translational response. A 3% damping value effectively reduces vibratory peaks without compromising structural integrity, suggesting a damping range of 3%–4% for future simulations to attenuate vibrations while avoiding over-design.

The RMS analysis further highlights damping's role in mitigating cumulative damage in sensitive components, emphasizing the need for precise damping control to prevent long-term damage.

The study suggests improvements in modeling fixation mechanisms, fluid-structure interactions, thermal loading, and launch ramp effects to enhance simulation accuracy and guide structural optimization for both small and large vehicles in future mission profiles.

Acknowledgements. Special thanks to my friends at CPL - UnB, for their contribution to the modeling of the thrust load.

Authorship statement. The authors hereby confirm that they are the sole liable persons responsible for the authorship of this work, and that all material that has been herein included as part of the present paper is either the property (and authorship) of the authors, or has the permission of the owners to be included here.

References

[1] L. Meirovitch. *Fundamentals of Vibrations*. McGraw-Hill, Boston, 2001.
[2] A. Preumont. *Vibration Control of Active Structures*. Springer, Dordrecht, 3rd edition, 2011.
[3] Chemical Propulsion Laboratory, University of Brasília. Desenvolvimento e teste de um motor foguete a propelentes híbridos fabricado por manufatura aditiva. Unpublished research project, not publicly available, 2025.
[4] D. N and L. Govindaraju. A study on shear frame structure by modal superposition method. *International Journal of Engineering Trends and Technology (IJETT)*, vol. 71, n. 2, pp. 247–252, 2023.
[5] C. Riso, S. Fransen, F. Mastroddi, G. Coppotelli, F. Trequattrini, and A. D. Vivo. Experimental validation of solid rocket motor damping models. *CEAS Space Journal*, vol. 10, n. 2, pp. 213–230, 2018.
[6] M. M. Rosso, A. Aloisio, J. Parol, G. C. Marano, and G. Quaranta. Intelligent automatic operational modal analysis. *Mechanical Systems and Signal Processing*, vol. 201, pp. 110669, 2023.